Title. *In vitro* function, assembly, and interaction of primary cell wall cellulose synthase homotrimers

Authors: Pallinti Purushotham, Ruoya Ho, Jochen Zimmer*

Affiliations: Department of Molecular Physiology and Biological Physics, University of Virginia School of Medicine, Charlottesville, VA 22903.
Howard Hughes Medical Institute.

*** For correspondence:** jz3x@virginia.edu

Abstract

Plant cell walls contain a meshwork of cellulose fibers embedded into a matrix of other carbohydrate and non-carbohydrate-based biopolymers. This composite material exhibits extraordinary properties, from stretchable and pliable cell boundaries to solid protective shells. Cellulose, a linear glucose polymer, is synthesized and secreted across the plasma membrane by cellulose synthase (CesA). Plants express several CesA isoforms, with different subsets necessary for primary and secondary cell wall biogenesis. The produced cellulose chains can be organized into fibrillar structures and fibrillogenesis likely requires the supramolecular organization of CesAs into pseudo sixfold symmetric complexes (CSCs). Here, we structurally and functionally characterize a set of soybean (Gm) CesA isoforms implicated in primary cell wall biogenesis. Cryogenic electron microscopy analyses of catalytically active GmCesA1, GmCesA3, and GmCesA6 reveal their assembly into homotrimeric complexes, stabilized by a cytosolic plant conserved region. Contrasting secondary cell wall CesAs, a peripheral position of the C-terminal transmembrane helix creates a large, lipid-exposed lateral opening of the enzymes' cellulose-conducting transmembrane channels. Co-purification experiments reveal that homotrimers of different CesA isoforms interact *in vitro* and that this interaction is independent of the enzymes' N-terminal cytosolic domains. Our data suggest that cross-isoform interactions are mediated by the class-specific region, which forms a hook-shaped protrusion of the catalytic domain at the cytosolic water-lipid interface. Further, inter-isoform interactions lead to synergistic catalytic activity, suggesting increased cellulose biosynthesis upon homotrimer interaction. Combined, our structural and biochemical data favor a model by which homotrimers of different CesA isoforms assemble into a microfibril-producing CSC.

Introduction

Cellulose is a versatile biopolymer and a fundamental building block of plant cell walls, like structural steel in the building industry. It is a linear polymer of glucose units that can be assembled into fibrillar structures. In plant cell walls, cellulose microfibrils are spun around the cell and integrated with a variety of other biopolymers to form the load bearing wall component ***(Turner and Kumar, 2018***).

Cellulose is synthesized by cellulose synthase (CesA), a membrane-integrated processive family-2 glycosyltransferase (GT) (***Lombard et al., 2014***). Remarkably, CesA synthesizes cellulose from UDP-activated glucose (UDP-Glc) and, during the synthesis reaction, translocates the polymer across the plasma membrane through a channel formed by its own membrane-spanning segment (***McNamara et al., 2015***). This multi-tasking requires functionally integrating a cytosolic catalytic GT domain with a membrane-spanning secretion channel.

Structural and functional analyses of bacterial and plant CesAs provided detailed insights into cellulose synthesis and secretion ***(Morgan et al., 2013; Purushotham et al., 2020; Zhang et al., 2021a***). Importantly, CesA binds one substrate molecule at a time, transfers a single glucosyl unit to the nascent cellulose chain in an elongation reaction, and, subsequently, translocates the elongated polymer into its channel (***Morgan et al., 2016***). Cellulose translocation positions the newly added terminal glucosyl unit (the acceptor) for another elongation reaction.

The mechanism of cellulose biosynthesis is evolutionarily conserved, from bacteria to land plants. Accordingly, the architectures of bacterial and plant CesAs share many structural features, including a cytosolic catalytic GT-A domain, an arrangement of three amphipathic interface helices (IF helices) that connect the GT domain with the TM region, and a cellulose secreting TM channel formed from at least six TM helices ***(Morgan et al., 2013; Purushotham et al., 2020; Zhang et al., 2021a***). A defining sequence motif of CesAs and related polysaccharide synthases is the QxxRW motif. The motif's Trp residue stabilizes the acceptor glucosyl unit right above the catalytic pocket, at the entrance to the TM channel (***Morgan et al., 2013***).

Plant CesAs contain specific domains absent in most bacterial homologs. These include an extended cytosolic N-terminus beginning with a RING-like region, a plant conserved region (PCR), as well as a class-specific region (CSR) (***Carpita, 2011; Purushotham et al., 2020; Wilson et al., 2021***). The CSR and PCR are integrated into peripheral extensions of the catalytic domain. Further, plants express different CesA isoforms at different developmental stages, of which certain subsets are necessary for primary and secondary cell wall formation ***(Persson et al., 2007; Taylor et al., 2003; Turner and Somerville, 1997***). Isoforms associated with primary cell wall formation include

77 CesA1, 3 and 6, while secondary cell wall CesA isoforms include CesA4, 7 and 8. The isoenzymes
78 vary the most within the CSR and the N-terminal domain.
79
80 Plants organize the individual cellulose polymers into micro and macro-fibrils ***(Kubicki et al.,***
81 ***2018; Turner and Kumar, 2018***). In a fibril, the cellulose polymers are aligned along the fiber
82 axis, leading to exceptionally stable biomaterials. Cellulose microfibrils likely originate from
83 supramolecular CesA complexes (CSCs). CSCs have been identified in different species and, in
84 land plants, appear primarily as pseudo sixfold symmetric membrane-integrated particles by freeze
85 fracture electron microscopy analyses ***(Herth and Weber, 1984; Kimura et al., 1999; Nixon et al.,***
86 ***2016***). The CSC repeat unit likely contains three CesA subunits, thereby accounting for 18 CesAs
87 per CSC and, accordingly, 18 cellulose polymers in a CSC-synthesized microfibril ***(Nixon et al.,***
88 ***2016; Turner and Kumar, 2018***).
89
90 Supporting this model, cryogenic electron microscopy (cryo EM) analyses of secondary cell wall
91 hybrid aspen CesA8 and rice CesA7 revealed homotrimeric complexes ***(Purushotham et al., 2020;***
92 ***Zhang et al., 2021a***). Each subunit produces a cellulose polymer and the trimer interface is formed
93 by the PCR and the C-terminal TM helix.
94
95 Genetic analyses demonstrated that different CesA isoforms are necessary for proper primary or
96 secondary cell wall formation (***Fagard et al., 2000; Turner and Somerville, 1997***). Further, co-
97 immunoprecipitation analyses suggested direct interactions between primary or secondary cell
98 wall CesA isoforms (***Gonneau et al., 2014; Taylor et al., 2003; Timmers et al., 2009***). Combined,
99 these observations nurtured the hypothesis that CesAs organize into heterotrimers of different
100 isoforms *in vivo*, which assemble into CSCs containing six copies of each isoenzyme.
101
102 To analyze the oligomerization and function of primary cell wall CesAs, we recombinantly
103 expressed and purified *Glycin max* (soybean) CesA1, CesA3 and CesA6. Cryo EM analyses of all
104 three CesA isoforms reveal the formation of homotrimeric complexes, similar to secondary cell
105 wall CesAs. The primary cell wall CesAs reveal a new position of transmembrane (TM) helix 7,
106 resulting in a cellulose translocation channel with a large lateral exit. All three CesAs are
107 catalytically active *in vitro*, with comparable catalytic rates and pH optima. *In vitro* interaction

108 studies demonstrate that homotrimers of different CesA isoforms interact, leading to synergistic
109 cellulose biosynthesis. Our results support a model by which CSCs consists of homotrimers of
110 different CesA isoforms.
111
112 **Results**
113
114 **Primary cell wall CesAs purify as high and low molecular weight species**
115 To biochemically and structurally characterize soybean primary cell wall CesAs, we followed a
116 similar heterologous expression protocol as previously described for hybrid aspen CesA8
117 (***Purushotham et al., 2020***). In short, the CesAs (***Figure supplement 1***) were expressed with N-
118 terminal poly-histidine tags in SF9 insect cells and purified by metal affinity and size exclusion
119 chromatography in the detergent glyco-diosgenin (GDN) (Materials and Methods). Size exclusion
120 chromatography separated all CesA isoforms into high and low molecular weight species (***Figure***
121 ***1*a-c**). Cryogenic and negative stain EM analyses identified these species as CesA trimers and
122 monomers, respectively, (***Purushotham et al., 2020***) (see below).
123
124 To test whether micelle-stabilized CesA trimers dissociate into monomers over time, the purified
125 CesA trimers were reinjected onto the size exclusion chromatography column after an overnight
126 incubation on ice. The reinjected material eluted as a trimeric complex, indicating that assembled
127 trimers are stable and do not interconvert with monomers within this timeframe (***Figure 1*a-c**). The
128 co-purifying monomers likely arise from incompletely assembled trimers or oligomer dissociation
129 during membrane solubilization.
130
131 **Primary cell wall CesAs are catalytically active *in vitro***
132 Cellulose biosynthetic activity was quantified by measuring the incorporation of ^{3}H-labeled
133 glucose into insoluble cellulose, followed by scintillation counting after removal of excess
134 substrate (see Materials and Methods) (***Purushotham et al., 2016***). As shown in ***Figure 1*d**, the
135 relative activities of the monomeric and trimeric CesA fractions are comparable for each isoform,
136 demonstrating that both species are catalytically active *in vitro*. Between the different isoforms,
137 CesA1 exhibits greatest product accumulation, whereas CesA3 and CesA6 yield about 25% of
138 product, compared to CesA1 (***Figure 1*d**). In all cases, the *in vitro* synthesized polymer is readily

139 degraded by a cellulase, indicating the formation of authentic cellulose. No product is obtained in
140 the presence of EDTA, in agreement with previous observations (***Purushotham et al., 2016***).
141
142 To further assess catalytic differences between the CesA isoforms, we determined their pH optima
143 for catalytic activity and turnover kinetics by titrating the substrate UDP-Glc and quantifying the
144 released UDP in an enzyme coupled reaction (see Materials and Methods) (***Figure 1*e *and* f**). All
145 CesA isoforms show greatest catalytic activity at neutral pH. CesA3 exhibits an activity optimum
146 at pH 7 with a sharp decline at pH 8 and 9. In contrast, the activities of CesA1 and CesA6 peak at
147 pH 8, with a slight decline at pH 9 (***Figure 1*e**). Further and consistent with the cellulose
148 quantification assay, CesA1 has an apparent Vmax of approximately 0.1 nmol/(sec mg), about four
149 and five times higher compared to CesA3 and CesA6, respectively (***Figure 1*f**). The affinities for
150 substrate binding range from 1.4 mM for CesA1 to 0.6 and 2.4 mM for CesA3 and CesA6,
151 respectively. Lastly, we analyzed inhibition of the isoforms by UDP, which competitively inhibits
152 CesA8 and other related enzymes ***(Gow and Selitrennikoff, 1984; Omadjela et al., 2013;***
153 ***Purushotham et al., 2016; Tlapak-Simmons et al., 2004)***. CesA1's apparent Ki for UDP is
154 roughly 0.8 mM, whereas this concentration is increased to about 1.2 to 1.5 mM for CesA6 and
155 CesA3, respectively (***Figure 1*g**).
156
157 **Primary and secondary cell wall CesAs assemble into homotrimers**
158 Cryo EM analyses of the high molecular weight fractions of the purified soybean CesAs (***Figure***
159 ***1*a-c**) revealed their organization into 3-fold symmetric homotrimers (***Figure 2*a - *figure***
160 ***supplements 2 and 3 and Supplement table 1***). For all isoforms, two-dimensional classification
161 identified trimeric particles similar to poplar CesA8 and rice CesA7 ***(Purushotham et al., 2020;***
162 ***Zhang et al., 2021a***). Particle classification in 3 dimensions followed by non-uniform and local
163 refinements generated cryo EM maps ranging in resolution from about 3.0 to 3.3 Å. We applied
164 3-fold symmetry (C3) during the refinement steps.
165
166 Overall, the CesAs contain a cytosolic catalytic domain that interacts with the channel-forming
167 TM region via three amphipathic IF helices (***Figure 2*b**). The helices surround the entrance to the
168 TM channel. The Trp residue of the conserved QxxRW motif, located in IF helix 2, sits at the
169 cytosolic channel entrance, right above the catalytic pocket, as previously observed for cellulose,

170 chitin and hyaluronan synthases ***(Chen et al., 2022; Maloney et al., 2022; Morgan et al., 2013;***
171 ***Ren et al., 2022***).
172
173 The CesA trimers are stabilized by the PCR domain that is inserted into the catalytic domain's GT-
174 A fold (***Lairson et al., 2008***) between β-strands 2 and 3. The PCR contains two anti-parallel α-
175 helices connected by a loop that folds back onto the helical pair (***Figure 2*c**). Within a trimer,
176 conserved residues of the PCR loop contact an equally conserved central region of PCR helix 2 of
177 a neighboring protomer. Specifically, the conserved DYLK motif (residue 434 to 437 in CesA6)
178 of the PCR loop interacts with residues 456 to 460 in PCR helix 2 of the neighboring subunit.
179 These residues belong to the conserved E/DYEEFKVR motif. The interprotomer contacts form a
180 salt bridge between Asp434 and Lys459, a hydrogen bond between Tyr435 and Glu456, and van
181 der Waals interactions between Leu436 and Ile445 with Glu456 in the opposing protomer. All
182 residue numbers refer to CesA6. No differences were observed at this PCR interfaces between the
183 CesA isoforms.
184
185 **The PCR trimer forms a positively charged interface**
186 As noted earlier for the secondary cell wall CesAs (***Purushotham et al., 2020***), the triangular PCR
187 arrangement in an assembled CesA complex positions the side chains of conserved Lys and Arg
188 residues towards the 3-fold symmetry axis. These residues, including Arg449, Lys452, and Arg453
189 in CesA6, are located in PCR helix 2. Also consistent with previous observations on CesA8 and
190 CesA7, the conserved positively charged residues coordinate an unidentified ligand on the
191 membrane distal and proximal side of the PCR triangle. For all three CesA isoforms, the ligands'
192 shapes are similar, suggesting that they represent the same small molecule (***Figure supplement***
193 ***3*c**). On the membrane proximal side, the density extends by about 9 Å towards the membrane,
194 consistent with a nucleotide bound in different poses, as previously suggested ***(Purushotham et***
195 ***al., 2020***).
196
197 **TM helix 7 sits at the periphery of the CesA trimer**
198 A notable structural difference between secondary and primary cell wall CesAs is the location of
199 the C-terminal TM helix 7. In hybrid aspen CesA8 and rice CesA7, the helix rests against TM
200 helices 5 and 6 of a neighboring protomer in the trimer, thereby contributing to its TM architecture

201 (***Figure 2*d**). In the soybean primary cell wall CesAs, however, the helix is more flexible, as
202 evidenced by weaker density maps. The helix is shifted to the periphery of the trimer, primarily
203 stabilized by intraprotomer contacts. TM helix 7 has been modeled for CesA3 and CesA6, while
204 its density is detectable but too discontinuous for modeling in CesA1 maps. In the new position,
205 TM helix 7 rests against TM helix 5 and the C-terminal segment of TM helix 3 of the same
206 protomer (***Figure 2*b *and* d**).
207
208 The displacement of TM helix 7 away from the channel architecture of the neighboring subunit
209 creates a large lateral lipid-exposed channel opening (***Figure 2*d**). This window is formed by the
210 N-terminal region of IF helix 3 and TM helices 4 and 6. About midway across the membrane, the
211 opening is roughly 6 Å wide, for example between Ile901 in TM helix 4 and Trp1018 in TM helix
212 6. This likely exposes the translocating nascent cellulose polymers to the hydrophobic milieu of
213 the lipid bilayer; yet no structured acyl chains (for example from detergent molecules) are observed
214 in this hydrophobic pocket. A similar lipid exposed polysaccharide translocation pathway has
215 recently been described for hyaluronan synthase (***Maloney et al., 2022***).
216
217 **A largely unstructured NTD and CSRs that extend from the CesA trimer's corners**
218 Although not resolved at high resolution, the N-terminal domain (NTD) of hybrid aspen CesA8
219 extends as a stalk into the cytosol along the trimer's symmetry axis (***Purushotham et al., 2020***).
220 Two-dimensional classification and a low resolution 3-dimensional reconstruction of GmCesA3
221 reveal a similar cytosolic extension (***Figure supplement 2***). The NTD is not resolved for
222 GmCesA1 and CesA6, suggesting that it adopts multiple conformations, with the stalk being one
223 of them.
224
225 Similarly, except for short helical segments at its N- and C-terminal ends, the CSR is largely
226 disordered in all CesA structures reported to date, consistent with its predicted flexibility
227 (***Scavuzzo-Duggan et al., 2018***). For GmCesA1, however, at lower contour levels, additional
228 density is observed extending from the corners of the CesA trimer (***Figure 2*e**). Viewed from the
229 cytosol, the extra density resembles a hook extending by about 20 Å clockwise and tangentially
230 along the trimer surface at the water-membrane interface. In this conformation, the CSR's N-

231 terminal conserved cysteine residue(s) postulated to be acylated (***Kumar et al., 2016***) is near the
232 membrane surface.
233
234 **CesAs co-purify with a nascent cellulose chain**
235 CesA is a processive GT that 'holds on' to the nascent cellulose polymer between elongation and
236 translocation steps. Studies on secondary cell wall CesAs demonstrated that recombinantly
237 expressed CesAs are catalytically active in the expression host. Accordingly, all experimentally
238 determined plant CesA structures reveal the presence of a cellooligosaccharide inside the
239 translocation channel. This is also observed for the primary cell wall soybean CesAs. Starting at
240 the active site, the terminal glucosyl units of the nascent chains are positioned at the acceptor site
241 next to the QxxRW motif's Trp residue (***Figure supplement 3*****b**). This is consistent with the
242 cellulose binding pose observed in bacterial CesA (Morgan *et al.*, 2016). Generally, the first two
243 glucosyl units are better resolved in the cryo EM maps, after which the densities become
244 discontinuous. Constraint by the map qualities, we only modeled di- and hexasaccharides into the
245 CesA3 and CesA6 structures, respectively.
246
247 **Interactions of homotrimers of different CesA isoforms**
248 We next tested whether CesA homotrimers of different isoforms interact *in vitro*. To this end, we
249 individually expressed and purified trimers of poly-His tagged CesA1 and CesA6 (His-CesA1 and
250 His-CesA6) and TwinStrep-tagged CesA1 and CesA3 (Strep-CesA1 and Strep-CesA3) (***Figure 3***).
251 Cross-isoform interactions were tested by tandem purifications over Ni-NTA and Strep-Tactin
252 affinity matrices. His-CesA1 can be distinguished from Strep-CesA3 by Coomassie stained SDS-
253 PAGE due to size differences, whereas all other species comigrate. Therefore, Western blotting
254 together with Coomassie stained SDS-PAGE was performed to evaluate all co-purification results.
255
256 An equimolar mixture of His-CesA1 and Strep-CesA3 was incubated for 180 min on ice and
257 sequentially purified using (1) Ni-NTA resin and (2) Strep-Tactin beads (***Figure 3*****a**). The
258 Coomassie stained SDS-PAGE resolves both CesA species in the initial mixture, after elution from
259 the Ni-NTA resin, as well as upon elution from the Strep-Tactin beads. The identity of the bands
260 as His-CesA1 and Strep-CesA3 was confirmed by Western blotting. We observed no non-specific
261 binding of His-CesA1 to Strep-Tactin beads or Strep-CesA3 to Ni-NTA resin (***Figure 3*****e**).

262

263 Similar experiments with combinations of Strep-CesA3 and His-CesA6 (***Figure 3*b**) and Strep-
264 CesA1 and His-CesA6 (***Figure 3c***) yielded comparable results, although the co-eluting species
265 cannot be distinguished by Coomassie staining alone, due to comigration. None of the species
266 showed detectable non-specific binding to the affinity resins in the absence of the corresponding
267 tags, (***Figure 3*e-g**).
268

269 As an additional control, we analyzed whether differently tagged homotrimers of the same isoform
270 also interact with each other. To this end, a mixture of His-CesA1 and Strep-CesA1 was subjected
271 to tandem affinity purification as described above (***Figure 3*d**). However, we failed to detect any
272 co-purification of Strep-CesA1 when applying Ni-NTA as the first affinity chromatography step.
273 Similar results were obtained for Strep- and His-tagged combinations of homotrimers of CesA3 or
274 CesA6 (***Figure supplements 4*a-d**). Qualitatively, our interaction data are consistent with
275 previously published co-immunoprecipitations of CesA isoforms ***(Gonneau et al., 2014; Timmers***
276 ***et al., 2009***).
277

278 Similar tandem purification experiments were also performed with the monomeric CesA fractions
279 obtained from size exclusion chromatography (***Figure 1*a-c**). As observed for the homotrimeric
280 complexes, monomeric His-CesA1 co-purifies with monomeric Strep-CesA3, demonstrating that
281 trimeric assemblies are not necessary for the observed interactions (***Figure supplements 4*e *and***
282 **f**).
283

284 **Homotrimers of different CesA isoforms assemble into clusters**

285 Negative stain electron microscopy of the individual CesA homotrimers revealed monodispersed
286 particle distributions for all three CesA isoforms (***Figure 4* a-c**). The size and shape of the particles
287 is consistent with CesA homotrimers as observed by cryo EM and remained unchanged over a
288 course of 4 days when the samples were stored on ice. In addition, all three homotrimeric isoforms
289 were combined and subjected to size exclusion chromatography after incubation overnight on ice.
290 Negative stain EM analysis of high molecular weight fractions eluting after the void volume
291 revealed CesA clusters of varying stoichiometries (***Figure 4*d**). The clusters likely arise from
292 trimer interactions in different orientations and range in diameter from about 50 to 100 nm. No

293 clustering was observed for the individual CesA isoforms alone, even after prolonged incubation
294 (4 days) on ice.
295
296 **CesA isoform interaction does not require the N-terminal domain**
297 The biological function of CesA's N-terminal domain (NTD) and CSR are unknown. While the
298 CSR is located at the corners of the CesA trimer (***Figure 2*e**), the NTD extends into the cytosol as
299 a stalk or adopts multiple conformations that are unresolved in cryo EM reconstructions (***Figure***
300 ***supplement 2***). The NTD's RING-like domain has been shown to form dimers and trimers *in vitro*
301 (***Kurek et al., 2002; Purushotham et al., 2020***), raising the possibility of forming inter-trimer
302 complexes accounting for the observed isoform interactions.
303
304 To test this hypothesis, N-terminally truncated constructs of CesA1 and CesA3 were expressed
305 and purified as described for the full-length variants. The constructs lack the first 259 (CesA1) and
306 242 (CesA3) residues yet purify as trimers (besides monomers) and exhibit *in vitro* catalytic
307 activity similar to the full-length constructs (***Figure 4*e**). A tandem affinity purification of a
308 mixture of the truncated His-CesA1 and Strep-CesA3 isoforms demonstrates their interaction *in*
309 *vitro*, as observed for the full-length enzymes (***Figure 4*f *and* g *and Figure 3*a**). This suggests that
310 the NTD is not required for inter-isoform interactions of CesAs *in vitro*.
311
312 **Synergistic cellulose biosynthesis**
313 We asked whether cross-isoform interactions of CesAs modulate their *in vitro* catalytic activities.
314 To this end, *in vitro* cellulose biosynthesis was quantified radiometrically from reactions
315 containing one CesA isoform at a constant concentration (20 µM) and increasing concentrations
316 of the other (1-20 µM). As a reference, cellulose biosynthetic activities were also determined for
317 each isoform alone at the concentrations used in the combined assays. As shown in Figure 5A-F,
318 for all isoform combinations, the measured activities exceed the theoretical activities (calculated
319 by adding the individually measured activities) at least one to two-fold, depending on the isoform
320 combination. This suggests synergistic cellulose biosynthesis in the presence of two different CesA
321 isoform trimers. Performing the titration experiment with samples of the same isoform does not
322 exhibit synergy, consistent with the lack of interactions of trimers of the same isoform (***Figure 5*g**
323 ***and 3d - figure supplement 5***).

Additionally, comparing the measured and additive activities obtained after combining all three CesA isoforms (at 6.6 µM each) reveals an experimental activity about 3-fold above the theoretical value. This activity level may arise from different dimeric arrangements of CesA trimers (1+3, 1+6, and 3+6) and/or the formation of trimeric complexes of different isoform trimers (1+3+6) (***Figure 5*****h**).

Activity measurements with the individual CesA isoforms suggest about 4-fold higher catalytic activity of CesA1 compared to CesA3 and CesA6 (***Figure 1*****d**). To test whether the observed synergistic effects are due to altered catalytic activity of only one isoform or both, one CesA isoform was inactivated after purification by incubation with the oxidant sodium tetrathionate ***(Tie et al., 2004***). While the inactivated CesAs exhibit activity levels comparable to EDTA-treated negative controls, they remain trimeric and interact with other isoforms as observed for the unmodified versions (***Figure supplement 6***). Inactivation could be due to modification of a conserved cysteine residue in CesA's catalytic pocket (such as Cys558 in CesA6).

Performing the above-described activity assays with pairs of inactive and active CesA trimers demonstrates that all three isoforms exhibit increased catalytic activity when combined with an inactive trimer of a different isoform (***Figure supplement 7***). This suggests that intertrimer interactions impact the catalytic activity of all isoforms, perhaps by altering the accessibility of the catalytic pocket (discussed below).

Discussion

A hallmark of plant cellulose biosynthesis is the formation and arrangement of cellulose microfibrils in the cell wall (***Zhang et al., 2021b)***. Prevailing models postulate the requirement of CesA supramolecular complexes (CSC) of at least three different isoforms ***(Newman et al., 2013; Turner and Kumar, 2018***) for proper cell wall biogenesis of primary and secondary cell walls. However, experimental evidence directly pinpointing isoform locations within a CSC or in its repeating unit is lacking.

354 Our attempts to isolate heterotrimeric complexes of co-expressed GmCesA1, GmCesA3 and
355 GmCesA6 failed, despite sufficient expression levels of all isoforms. Thus, we shifted our attention
356 to characterizing the isoforms individually. All three isoforms can be purified as catalytically
357 active homotrimeric species. Trimerization involves the same structural motifs identified in CesA8
358 and CesA7, primarily the cytosolic PCR domain. Because the PCR is highly conserved across the
359 three isoforms, the apparent failure of heterotrimer formation may be due to subtle differences in
360 sequence and shape complementarity of the isoforms.
361
362 Differently arranged TM helices in primary cell wall CesAs compared to CesA8 and CesA7 create
363 a large lateral window in the cellulose secretion channel. The window opens towards the trimer's
364 3-fold symmetry axis. While the biological function of this window is unclear, it could enable the
365 lateral release of the glucan chains towards the center of the complex, thereby facilitating the
366 alignment of the nascent glucan chains into a protofibril.
367
368 Our *in vitro* CesA interaction studies replicate previous *in vivo* co-immunoprecipitation results on
369 primary and secondary cell wall CesAs (***Gonneau et al., 2014; Timmers et al., 2009***). The robust
370 interaction of different CesA isoform trimers supports their physiological significance. In a
371 detergent solubilized state, the individual CesA trimers are not confined to the same plane, as
372 would be the case in a biological membrane. Thus, the *in vitro* observed interactions lead to
373 clustering of the trimers, instead of an ordered array into symmetric particles. Isoform interactions
374 do not require the N-terminal domain containing the dimerization-prone RING-like domain.
375 Therefore, we propose the CSR domain as the primary mediator of trimer-trimer interactions
376 (***Figure 6***), in agreement with earlier interpretations (***Sethaphong et al., 2013; Singh et al., 2020***).
377 This model is supported by the CSR's hook-like extension from the CesA trimer. We assume
378 distinct binding sites for two 'non-like' isoforms within a CSR. A dimeric complex of, for example
379 CesA1 and CesA3, would then only be able to interact with CesA6, thereby explaining the
380 functional importance of three CesA isoforms. This model can be modified by postulating multiple
381 binding sites for the same 'non-like; isoform or even a 'like' isoform to account for possible CSC
382 configurations of two or one isoform. Because trimers of the same isoform do not interact in vitro,
383 CSC models relying on interactions between the same CesA isoforms across the repeat units are
384 unlikely (***Figure 6***).

385

386 Because the CSR is a structurally flexible domain ***(Scavuzzo-Duggan et al., 2018***) that likely
387 occupies a large volume at the periphery of the catalytic domain, it is possible that it impacts
388 nucleotide binding to or exchange at the active site. The CSR could be repositioned upon
389 interaction with another isoform, which in turn could increase catalytic activity and account for
390 the observed synergistic effects.

391

392 Lastly, the biological functions of the different CesA isoforms are currently unknown. Requiring
393 different isoforms to form a functional CSC could provide regulatory control over the cellulosic
394 material that is deposited in the cell wall. It is conceivable that CesA trimers function alongside
395 fully assembled CSCs in the plasma membrane, thereby producing micro- and protofibrils (from
396 CSCs and trimers, respectively) that may interact. Accordingly, controlling the ability of the CesAs
397 to assemble into CSCs by regulating the isoform composition in the plasma membrane may allow
398 tailoring the fibril-to-protofibril ratio and thereby wall properties. Addressing these questions will
399 require detailed studies of the oligomerization and distribution of cellulose depositing CesA
400 complexes in the plasma membrane.

401 **Materials and methods**

402

403 **GmCesA protein expression and purification**

404

405 **Cloning**

406 The primary cell wall CesA1, 3 and 6 genes from soybean were synthesized (Gene Universal) with
407 an N-terminal 12x His-tag coding sequence and cloned into *Not*I and *Hind*III restriction sites in
408 the pACEBac1vector. The N-terminally TwinStrep-tagged CesA1 and CesA3 constructs were
409 generated by QuikChange mutagenesis from the pACEBac1-12xHisCesA vectors. The N-
410 terminally deleted GmCesA constructs (ΔNCesAs) were generated by PIPE cloning from the full-
411 length constructs, resulting in plasmids pACEBac1-ΔNCesA1R260, pACEBac1-ΔNCesA3V243,
412 and pACEBac1-ΔNCesA6M248.

413

414 **Virus generation**

415 An aliquot of 3 µL of 100 ng/µL pACEBac1-CesA plasmid was used for transformation into 50
416 µL chemical-competent DH10MultiBacTurbo *E. coli* cells. Bacmids were isolated from white
417 colonies on a Bluo-Gal agar plate and transfected into *Spodoptera frugiperda* 9 (SF9) cells. P0,
418 P1 and P2 baculovirus was generated according to the Joint Centre for innovative membrane
419 protein technologies (JCIMPT) protocol.
420
421 **Protein expression and purification**
422 For GmCesAs expression, SF9 insect cells were infected with a baculovirus at a density of 3 M
423 cells per mL and grown at 27 °C for 48-72 h in an orbital shaker. Cells were then harvested by
424 centrifugation at 5,000xg for 10 min at 4 °C. Cell pellets were resuspended in buffer A (20 mM
425 Tris-HCl, pH 7.5, 100 mM NaCl, 5 mM sodium phosphate, 5 mM sodium citrate, 1 mM TCEP, 1
426 µM leupeptin, 1 µM pepstatin, 0.5 µM aprotinin, 1 mM AEBSF, 100 µM bestatin, 10 µM E-64
427 and 5 mM Benzamidine HCl) containing 1% Lauryl Maltose Neopentyl Glycol (LMNG, Anatrace)
428 and 0.2% cholesteryl hemisuccinate (CHS, Anatrace) and lysed in a glass dounce homogenizer (~
429 30 strokes). The lysate was solubilized at 4°C for 1 h in a rotator shaker. After separation of
430 insoluble material by centrifugation at 204,709 x g for 30 min, 5 mL of Ni-NTA resin (HisPur Ni-
431 NTA Resin, Thermo scientific) was added to the supernatant and incubated for 1 h at 4 °C in a
432 rotator shaker. The resin was then sequentially washed, wash 1 and wash 2, with 10 column
433 volumes each of buffer A containing 40 mM imidazole, 0.02% glyco-diosgenin (GDN, Anatrace),
434 followed by 10 column volumes of buffer A containing 1 M NaCl and 0.02% GDN (wash 3). The
435 final wash step (wash 4) was with buffer A containing 0.02% GDN and 60 mM imidazole. The
436 GmCesAs were eluted with five column volumes of buffer A containing 0.02% GDN and 400 mM
437 imidazole.
438
439 The TwinStrep tagged GmCesAs was affinity purified by incubating the membrane extract with
440 Strep-Tactin sepharose at 4 °C for 1 h in a rotator shaker. After batch binding, the resin was packed
441 into a gravity flow column and washed as mentioned above for Ni-NTA affinity column except
442 the buffers lacked imidazole. The TwinStrep-tagged CesA was eluted using 10 column volumes
443 of buffer A containing 0.02% GDN and 5 mM desthiobiotin.
444

445 His- and TwinStrep-tagged GmCesAs were further purified by size-exclusion chromatography
446 (SEC) using Superose 6 Increase 10/300 GL column (Cytiva) equilibrated in buffer A containing
447 0.02% GDN without any protease inhibitors. The purified GmCesA trimers and monomers were
448 immediately used for activity assays and pulldown experiments or flash-frozen in liquid nitrogen
449 and stored at -80°C.
450
451 **CesA-CesA pull-down assays**
452 After SEC, either the trimeric or monomeric fractions of His-CesA and TwinStrep-CesA were
453 pooled and used for tandem affinity chromatography using Ni-NTA and Strep-Tactin sepharose
454 beads. His-CesA1 and TwinStrep-CesA3 trimers were mixed at 150 µg/mL concentration and
455 incubated at 4 °C for 3 h. The mixture was first loaded onto 200 µL bed volume Ni-NTA beads
456 for 1 h at 4 °C in the presence of 20 mM imidazole. After collecting the flowthrough, the beads
457 were washed with 10 column volumes of buffer A containing 0.02% GDN and 20 mM imidazole
458 for 3 washes followed by elution in 5 column volumes of buffer A containing 0.02% GDN and
459 400 mM imidazole.
460
461 The Ni-NTA eluted material was next bound to 200 µL Strep-Tactin sepharose beads for 1 h at
462 4 °C in a rotator shaker. After batch binding, the beads were packed into a gravity flow column.
463 The flow-through was collected and the column was subsequently washed 3-times with 10 column
464 volumes of buffer A containing 0.02% GDN. Bound proteins were eluted with buffer A containing
465 0.02% GDN and 5 mM desthiobiotin. All fractions were analyzed by SDS-polyacrylamide gel
466 electrophoresis (SDS-PAGE) and Western blotting using anti-His (Qiagen) and anti-strep
467 (MilliporeSigma) primary antibodies and an IRDye800-coupled anti-mouse secondary antibody
468 (Rockland) for detection.
469
470 The same protocol was used to study the interactions of CesA1 and CesA6 or CesA3 and CesA6
471 using Strep-tagged CesA1 and His-tagged CesA6, Strep-tagged CesA3 and His-tagged CesA6,
472 respectively. Control binding experiments were performed by loading the His-tagged CesA
473 species onto Strep-Tactin sepharose beads and the Strep-tagged CesAs onto the Ni-NTA beads. In
474 each case, the beads were washed as described above.
475

476 **Inactivation of CesA**

477 CesA was inactivated by treating CesA trimers with 10 mM sodium tetrathionate overnight at room
478 temperature (24 °C). The treated sample was purified over a size exclusion column to remove the
479 excess sodium tetrathionate. Binding experiments with inactivated and untreated CesAs were
480 performed using Ni-NTA beads as described above.

481

482 **GmCesA activity assay**

483 Freshly purified or aliquots of flash-frozen enzyme thawed on ice were used for activity assays. In
484 general, activity assays were performed as described earlier ***(Carpita, 2011; Purushotham et al.,***
485 ***2020; Wilson et al., 2021***). Radiometric quantification of *in vitro* synthesized cellulose was
486 performed by combining 5 µM GmCesA, 5 mM UDP-glucose (UDP-Glc), and 0.25 µCi UDP-
487 [^{3}H]-Glc in buffer containing 20 mM Tris-HCl, pH 7.5, 100 mM NaCl, 20 mM $MgCl_2$, 5 mM
488 sodium phosphate, 5 mM sodium citrate,1 mM TCEP. The reaction mixtures were incubated for
489 45 min at 37°C. After incubation, the entire reaction mixture was spotted on Whatman Grade 3MM
490 chromatography paper. Free substrate was removed by descending paper chromatography in 60%
491 ethanol. The radioactivity retained at the origin was quantified by scintillation counting.

492

493 The pH optima of GmCesAs were determined by incubating the CesAs in MMT buffer, consisting
494 of DL-malic acid, MES and Tris base in the molar ratios 1:2:2-DL-malic acid:MES:Tris base. The
495 desired pH was adjusted with NaOH or HCl. Activity assay was performed as mentioned above in
496 triplicate from two biological replicates.

497

498 Cellulase digestions were performed by adding 5 U of endo-β-1,4-glucanase (*Trichoderma*
499 *longibrachiatum*; Megazyme: E-CELTR) directly to the reaction mixture. Post *in vitro* synthesis
500 reaction, cellulase treatment was performed for 3 h at 37°C. Cellulose quantification by
501 scintillation counting was performed as mentioned above to quantify the product.

502

503 Steady-state kinetic analyses were performed in triplicate using the UDP-Glo Glycosyltransferase
504 Assay kit (Promega) to monitor the released UDP according to the manufacturer's instructions.
505 For measuring enzyme kinetics, the reaction mixtures containing 5 µM GmCesA, 0.005-5 mM
506 UDP-Glc were added to 20 mM Tris-HCl buffer (pH 7.5), 100 mM NaCl, 5 mM sodium phosphate,

507 5 mM sodium citrate, 20 mM $MgCl_2$ and incubated in a final volume of 25 µl for 45 min at
508 37°C. The reaction mixture was mixed with an equal amount of UDP-Glo reagent in a 96-well
509 Nunclon Delta-Treated flat-bottom microplate (Thermo Scientific) and incubated for 1 h at room
510 temperature before measuring luminescence using a GloMax Explorer plate reader (Promega). A
511 standard curve was used for quantification of the UDP produced. Kinetic values were obtained
512 using the nonlinear regression function in GraphPad Prism.
513
514 **GmCesA UDP inhibition assays**
515 UDP inhibition was analyzed using radiometric quantification of *in vitro* synthesized cellulose, as
516 described above by titrating 0.01-7.5 mM UDP in the reaction. Substrate concentrations for the
517 individual reactions matched the estimated Km values: CesA1: 1.4 mM; CesA3: 0.5 mM; CesA6:
518 2.3 mM. Inhibition constants (Ki) for each CesA were obtained by analyzing the data using
519 GraphPad Prism software.
520
521 **Synergistic cellulose biosynthesis**
522 Activity synergism between different CesA isoform trimers were studied by mixing two CesA
523 isoforms, one at a constant concentration of 20 µM and one at increasing concentrations from 1-
524 20 µM. The activities of the individual isoforms at the respective concentrations were also
525 measured. *In vitro* synthesized cellulose was quantified by scintillation counting, as described
526 above.
527
528 **EM grid preparation and data collection**
529 After size exclusion chromatography, the freshly purified protein fractions were pooled. The
530 protein quality was monitored by negative stain EM. The proteins were diluted to 0.01 mg/mL and
531 4 µL was applied to a glow discharged Formvar/Carbon grid (Electron Microscopy Sciences) for
532 30 s, followed by 2x washes with 4 µL H_2O. The grid was negatively stained with 4 µl 0.75%
533 Uranyl Formate (UF) in H_2O for 30 s. Excess UF was removed by blotting with filter paper and
534 the grid was air dried. Images were taken on a Tecnai F20 at Macromolecular Electron Microscopy
535 Core (MEMC) facility at the University of Virginia.
536

537 For cryo grid preparation, the protein samples were concentrated to ~3 mg/mL (based on UV
538 absorbance). Samples of 2.5 µL were applied to a C-flat 300 mesh 1.2/1.3 copper grids (Electron
539 Microscopy Sciences), glow-discharged in the presence of amylamine at 25 mA for 45 s, and
540 blotted with a Vitrobot Mark IV (FEI, Thermo Fisher Scientific) with force 4 for 6 s at 4°C, 100%
541 humidity, and frozen in liquid ethane.
542
543 Cryo EM data were collected at the MEMC at the University of Virginia on a Titan Krios
544 microscope operated at 300 keV and equipped with a Gatan K3 direct electron detector positioned
545 post a Gatan Quantum energy filter. Total ~6000 movies were collected from 2 grids in counting
546 mode at a magnification of 81K, pixel size of 1.08 Å, and defocus range from -2.2 to -1.2 µm with
547 step size of 0.2 µm. The total dose was 50 $e^-/Å^2$. Movies with 40 frames were collected at 5.17
548 s/movie rate.
549
550 **Cryo EM data processing**
551 Cryo EM data processing was done in cryoSPARC v4 (***Punjani et al., 2017***). The general
552 workflow is described in *SI Appendix*, Fig. S2. Based on improved map qualities, all volumes were
553 generated imposing 3-fold symmetry (C3). Maps generated without symmetry assignment (C1)
554 were used to visualize the unidentified ligand coordinated by the PCR domains at the particle's
555 symmetry axis. Initial protein models were generated in AlphaFold and manually adjusted in
556 Chimera and Coot (***Emsley and Cowtan, 2004; Pettersen et al., 2004***). Models were refined in
557 Phenix.refine (***Afonine et al., 2012***). The following regions were omitted from the constructs due
558 to weak or missing map density: CesA1:1-260 (NTD), 654-717 (CSR), 954-978 (gating loop),
559 1064-1078 (C term); CesA3: 1-251 (NTD), 648-712 (CSR), 946-974 (gating loop), 1032-1079 (C
560 term and TM 7); and CesA6: 1-248 (NTD), 646-712 (CSR), 952-971 (gating loop), 1058-1078 (C
561 term). Structural representations were generated in ChimeraX or Pymol ***(Pettersen et al., 2021;***
562 ***Pymol***).
563
564 **Data availability**
565 PDB coordinates and cryo EM maps have been deposited at the PDB with accessing codes 8VHZ,
566 8VHT, and 8VIO.
567

Funding

This work was supported in part by BASF (CesA cloning, expression, and structure determination) and the Center for LignoCellulose Structure and Formation (CLSF, biochemical and interaction studies). CLSF is an Energy Frontier Research Center funded by the U.S. Department of Energy, Office of Science, Basic Energy Sciences (award DESC0001090). R.H. and J.Z. are supported by NIH grant R35GM144130 awarded to J.Z. J.Z. is an investigator of the Howard Hughes Medical Institute.

Author contribution

P.P. purified all CesAs and performed all activities assays. R.H. prepared cryo EM grids and collected data. J.Z assisted in data processing and model building. All authors contributed to manuscript preparation.

Acknowledgements

We are grateful to Kelly Dryden and Michael Purdy of UVA's Macromolecular Electron Microscopy Core (MEMC) facility for support during EM data collection.

Competing interest

The authors declare no conflict of interests exist.

590 **References**
591
592 **Afonine, P.V., Grosse-Kunstleve, R.W., Echols, N., Headd, J.J., Moriarty, N.W., Mustyakimov,**
593 **M., Terwilliger, T.C., Urzhumtsev, A., Zwart, P.H., and Adams, P.D.** (2012). Towards automated
594 crystallographic structure refinement with phenix.refine. Acta Crystallogr D Biol Crystallogr
595 **68**:352-367. 10.1107/S0907444912001308.
596 **Carpita, N.C.** (2011). Update on mechanisms of plant cell wall biosynthesis: how plants make
597 cellulose and other (1->4)-beta-D-glycans. Plant Physiol **155**:171-184. 10.1104/pp.110.163360.
598 **Chen, W., Cao, P., Liu, Y., Yu, A., Wang, D., Chen, L., Sundarraj, R., Yuchi, Z., Gong, Y.,**
599 **Merzendorfer, H., et al.** (2022). Structural basis for directional chitin biosynthesis. Nature
600 **610**:402-408. 10.1038/s41586-022-05244-5.
601 **Emsley, P., and Cowtan, K.** (2004). Coot: model-building tools for molecular graphics. Acta
602 Crystallogr D Biol Crystallogr **60**:2126-2132. 10.1107/S0907444904019158.
603 **Fagard, M., Desnos, T., Desprez, T., Goubet, F., Refregier, G., Mouille, G., McCann, M., Rayon,**
604 **C., Vernhettes, S., and Höfte, H.** (2000). encodes a cellulose synthase required for normal cell
605 elongation specifically in roots and dark-grown hypocotyls of arabidopsis. Plant Cell **12**:2409-
606 2423. DOI 10.1105/tpc.12.12.2409.
607 **Gonneau, M., Desprez, T., Guillot, A., Vernhettes, S., and Hofte, H.** (2014). Catalytic subunit
608 stoichiometry within the cellulose synthase complex. Plant Physiol **166**:1709-1712.
609 10.1104/pp.114.250159.
610 **Gow, L.A., and Selitrennikoff, C.P.** (1984). Chitin Synthetase of Neurospora-Crassa - Inhibition
611 by Nikkomycin, Polyoxin-B, and Udp. Curr Microbiol **11**:211-216. Doi 10.1007/Bf01567162.
612 **Herth, W., and Weber, G.** (1984). Occurrence of the Putative Cellulose-Synthesizing Rosettes in
613 the Plasma-Membrane of Glycine-Max Suspension-Culture Cells. Naturwissenschaften **71**:153-
614 154. Doi 10.1007/Bf01137780.
615 **Kimura, S., Laosinchai, W., Itoh, T., Cui, X., Linder, C.R., and Brown, R.M.J.** (1999). Immunogold
616 labeling of rosette terminal cellulose-synthesizing complexes in the vascular plant Vigna
617 angularis. Plant Cell **11**:2075-2086. 10.1105/tpc.11.11.2075.
618 **Kubicki, J.D., Yang, H., Sawada, D., O'Neill, H., Oehme, D., and Cosgrove, D.** (2018). The Shape
619 of Native Plant Cellulose Microfibrils. Sci Rep **8**:13983. 10.1038/s41598-018-32211-w.
620 **Kumar, M., Wightman, R., Atanassov, I., Gupta, A., Hurst, C.H., Hemsley, P.A., and Turner, S.**
621 (2016). S-Acylation of the cellulose synthase complex is essential for its plasma membrane
622 localization. Science **353**:166-169. 10.1126/science.aaf4009.
623 **Kurek, I., Kawagoe, Y., Jacob-Wilk, D., Doblin, M., and Delmer, D.** (2002). Dimerization of
624 cotton fiber cellulose synthase catalytic subunits occurs via oxidation of the zinc-binding
625 domains. Proc Natl Acad Sci U S A **99**:11109-11114. 10.1073/pnas.162077099.
626 **Lairson, L.L., Henrissat, B., Davies, G.J., and Withers, S.G.** (2008). Glycosyltransferases:
627 structures, functions, and mechanisms. Annu Rev Biochem **77**:521-555.
628 10.1146/annurev.biochem.76.061005.092322.
629 **Larkin, M.A., Blackshields, G., Brown, N.P., Chenna, R., McGettigan, P.A., McWilliam, H.,**
630 **Valentin, F., Wallace, I.M., Wilm, A., Lopez, R., et al.** (2007). Clustal W and Clustal X version
631 2.0. Bioinformatics **23**:2947-2948. 10.1093/bioinformatics/btm404.

632 **Lombard, V., Ramulu, H.G., Drula, E., Coutinho, P.M., and Henrissat, B.** (2014). The
633 carbohydrate-active enzymes database (CAZy) in 2013. Nucleic Acids Res **42**:D490-D495.
634 10.1093/nar/gkt1178.
635 **Maloney, F.P., Kuklewicz, J., Corey, R.A., Bi, Y.C., Ho, R.Y., Mateusiak, L., Pardon, E., Steyaert,**
636 **J., Stansfeld, P.J., and Zimmer, J.** (2022). Structure, substrate recognition and initiation of
637 hyaluronan synthase. Nature **604**:195-201. 10.1038/s41586-022-04534-2.
638 **McNamara, J.T., Morgan, J.L.W., and Zimmer, J.** (2015). A molecular description of cellulose
639 biosynthesis. Annu Rev Biochem **84**:17.11-17.27.
640 **Morgan, J., Strumillo, J., and Zimmer, J.** (2013). Crystallographic snapshot of cellulose synthesis
641 and membrane translocation. Nature **493**:181-186.
642 **Morgan, J.L., McNamara, J.T., Fischer, M., Rich, J., Chen, H.M., Withers, S.G., and Zimmer, J.**
643 (2016). Observing cellulose biosynthesis and membrane translocation in crystallo. Nature
644 **531**:329-334. 10.1038/nature16966.
645 **Newman, R.H., Hill, S.J., and Harris, P.J.** (2013). Wide-angle x-ray scattering and solid-state
646 nuclear magnetic resonance data combined to test models for cellulose microfibrils in mung
647 bean cell walls. Plant Physiol **163**:1558-1567. 10.1104/pp.113.228262.
648 **Nixon, B.T., Mansouri, K., Singh, A., Du, J., Davis, J.K., Lee, J.G., Slabaugh, E., Vandavasi, V.G.,**
649 **O'Neill, H., Roberts, E.M., et al.** (2016). Comparative Structural and Computational Analysis
650 Supports Eighteen Cellulose Synthases in the Plant Cellulose Synthesis Complex. Sci Rep
651 **6**:28696. 10.1038/srep28696.
652 **Omadjela, O., Narahari, A., Strumillo, J., Mélida, H., Mazur, O., Bulone, V., and Zimmer, J.**
653 (2013). BcsA and BcsB form the catalytically active core of bacterial cellulose synthase sufficient
654 for in vitro cellulose synthesis. Proc Natl Acad Sci U S A **110**:17856-17861.
655 10.1073/pnas.1314063110.
656 **Persson, S., Paredez, A., Carroll, A., Palsdottir, H., Doblin, M., Poindexter, P., Khitrov, N.,**
657 **Auer, M., and Somerville, C.R.** (2007). Genetic evidence for three unique components in
658 primary cell-wall cellulose synthase complexes in Arabidopsis. Proc Natl Acad Sci USA
659 **104**:15566-15571. DOI 10.1073/pnas.0706592104.
660 **Pettersen, E.F., Goddard, T.D., Huang, C.C., Couch, G.S., Greenblatt, D.M., Meng, E.C., and**
661 **Ferrin, T.E.** (2004). UCSF Chimera--a visualization system for exploratory research and analysis. J
662 Comput Chem **25**:1605-1612. 10.1002/jcc.20084.
663 **Pettersen, E.F., Goddard, T.D., Huang, C.C., Meng, E.C., Couch, G.S., Croll, T.I., Morris, J.H.,**
664 **and Ferrin, T.E.** (2021). UCSF ChimeraX: Structure visualization for researchers, educators, and
665 developers. Protein science : a publication of the Protein Society **30**:70-82. 10.1002/pro.3943.
666 **Punjani, A., Rubinstein, J.L., Fleet, D.J., and Brubaker, M.A.** (2017). cryoSPARC: algorithms for
667 rapid unsupervised cryo-EM structure determination. Nat Methods **14**:290-296.
668 10.1038/nmeth.4169.
669 **Purushotham, P., Ho, R., and Zimmer, J.** (2020). Architecture of a catalytically active
670 homotrimeric plant cellulose synthase complex. Science **369**:1089-1094.
671 **Purushotham, P., Cho, S.H., Diaz-Moreno, S.M., Kumar, M., Nixon, B.T., Bulone, V., and**
672 **Zimmer, J.** (2016). A single heterologously expressed plant cellulose synthase isoform is
673 sufficient for cellulose microfibril formation in vitro. Proc Natl Acad Sci U S A **113**:11360-11365.
674 10.1073/pnas.1606210113.
675 Pymol The PYMOL Molecular Graphics System.

676 **Ren, Z., Chhetri, A., Guan, Z., Suo, Y., Yokoyama, K., and Lee, S.Y.** (2022). Structural basis for
677 inhibition and regulation of a chitin synthase from Candida albicans. Nat Struct Mol Biol **29**:653-
678 664. 10.1038/s41594-022-00791-x.
679 **Scavuzzo-Duggan, T.R., Chaves, A.M., Singh, A., Sethaphong, L., Slabaugh, E., Yingling, Y.G.,**
680 **Haigler, C.H., and Roberts, A.W.** (2018). Cellulose synthase "class specific regions' are
681 intrinsically disordered and functionally undifferentiated. J Integr Plant Biol **60**:481-497.
682 10.1111/jipb.12637.
683 **Sethaphong, L., Haigler, C., Kubicki, J., Zimmer, J., Bonetta, D., DeBolt, S., and Yingling, Y.**
684 (2013). Tertiary model of a plant cellulose synthase. Proc Natl Acad Sci U S A **110**:7512-7517.
685 10.1073/pnas.1301027110.
686 **Singh, A., Kwansa, A.L., Kim, H.S., Williams, J.T., Yang, H., Li, N.K., Kubicki, J.D., Roberts, A.W.,**
687 **Haigler, C.H., and Yingling, Y.G.** (2020). In silico structure prediction of full-length cotton
688 cellulose synthase protein (GhCESA1) and its hierarchical complexes. Cellulose **27**:5597-5616.
689 **Taylor, N.G., Howells, R.M., Huttly, A.K., Vickers, K., and Turner, S.R.** (2003). Interactions
690 among three distinct CesA proteins essential for cellulose synthesis. Proc Natl Acad Sci USA
691 **100**:1450-1455. 10.1073/pnas.0337628100.
692 **Tie, J.K., Jin, D.Y., Loiselle, D.R., Pope, R.M., Straight, D.L., and Stafford, D.W.** (2004). Chemical
693 modification of cysteine residues is a misleading indicator of their status as active site residues
694 in the vitamin K-dependent γ-glutamyl carboxylation reaction. J Biol Chem **279**:54079-54087.
695 10.1074/jbc.M408945200.
696 **Timmers, J., Vernhettes, S., Desprez, T., Vincken, J.P., Visser, R.G., and Trindade, L.M.** (2009).
697 Interactions between membrane-bound cellulose synthases involved in the synthesis of the
698 secondary cell wall. FEBS Lett **583**:978-982. 10.1016/j.febslet.2009.02.035.
699 **Tlapak-Simmons, V.L., Baron, C.A., and Weigel, P.H.** (2004). Characterization of the purified
700 hyaluronan synthase from Streptococcus equisimilis. Biochemistry **43**:9234-9242.
701 10.1021/bi049468v.
702 **Turner, S., and Kumar, M.** (2018). Cellulose synthase complex organization and cellulose
703 microfibril structure. Philos T R Soc A **376**ARTN 20170048
704 10.1098/rsta.2017.0048.
705 **Turner, S.R., and Somerville, C.R.** (1997). Collapsed xylem phenotype of Arabidopsis identifies
706 mutants deficient in cellulose deposition in the secondary cell wall. Plant Cell **9**:689-701. DOI
707 10.1105/tpc.9.5.689.
708 **Waterhouse, A.M., Procter, J.B., Martin, D.M., Clamp, M., and Barton, G.J.** (2009). Jalview
709 Version 2--a multiple sequence alignment editor and analysis workbench. Bioinform **25**:1189-
710 1191. 10.1093/bioinformatics/btp033.
711 **Wilson, T.H., Kumar, M., and Turner, S.R.** (2021). The molecular basis of plant cellulose
712 synthase complex organisation and assembly. Biochem Soc T **49**:379-391.
713 10.1042/Bst20200697.
714 **Zhang, X.N., Xue, Y., Guan, Z.Y., Zhou, C., Nie, Y.F., Men, S., Wang, Q., Shen, C.C., Zhang, D.L.,**
715 **Jin, S.X., et al.** (2021a). Structural insights into homotrimeric assembly of cellulose synthase
716 CesA7 from Gossypium hirsutum. Plant Biotechnol J **19**:1579-1587. 10.1111/pbi.13571
717 **Zhang, Y., Yu, J.Y., Wang, X., Durachko, D.M., Zhang, S.L., and Cosgrove, D.J.** (2021b).
718 Molecular insights into the complex mechanics of plant epidermal cell walls. Science **372**:706-+.
719 10.1126/science.abf2824.

720 **Figures and figure legends**

721

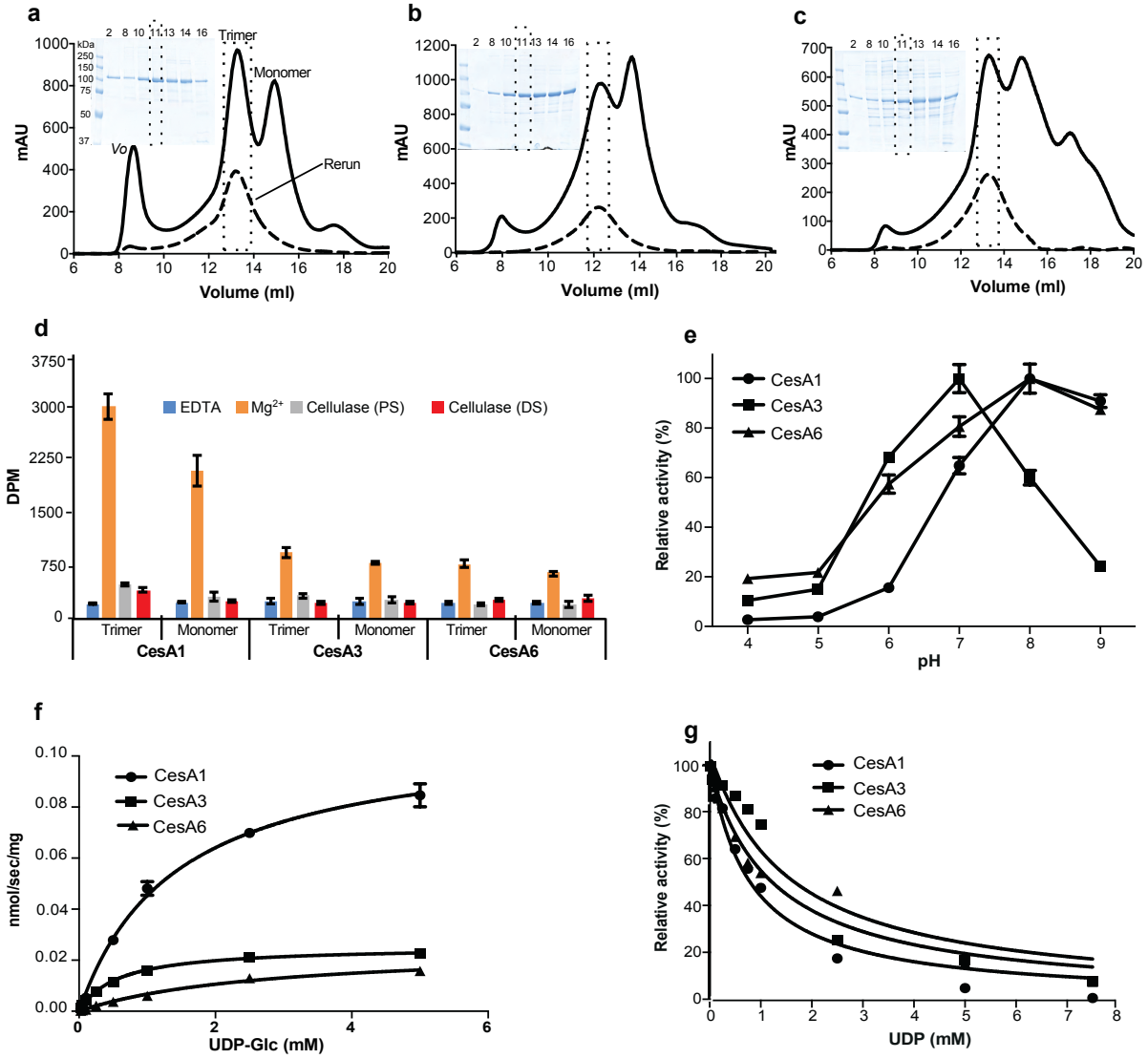

722

723

724 **Figure 1.** Functional characterization of *Glycine max* primary cell wall CesAs. From **(a-c)**
725 Analytical size exclusion chromatography (Superose 6 Increase) of GmCesA1 **(a)**, GmCesA3 **(b)**,
726 and GmCesA6 **(c)**. Void volume (*Vo*) and trimer and monomer peaks are marked. A rerun of the
727 trimer fraction for each species is shown as a dashed profile. Inset: Coomassie-stained SDS-
728 polyacrylamide gel electrophoresis of the indicated elution volumes. **(d)** Catalytic activity of the
729 purified CesAs. ^{3}H-labeled cellulose synthesized by trimeric and monomeric species was degraded
730 with cellulase, followed by quantification by scintillation counting. (DS) and (PS) indicate
731 cellulase treatments during and after the synthesis reaction, respectively. DPM: disintegrations per

732 minute. **(e)** pH optima for catalytic activity of CesA1, 3 and 6. Activities are normalized to the
733 highest activity for each isoform. **(f)** Kinetic analyses of CesAs by titrating UDP-Glc and
734 quantification of the released UDP using an UDP-Glo assay kit. **(g)** UDP inhibits CesAs. Cellulose
735 biosynthesis in the presence of 1.4, 0.5, and 2.3 mM UDP-Glc for GmCesA1, 3, and 6, respectively,
736 and the indicated increasing concentrations of UDP. Product yields in the absence of UDP were
737 set as 100 %. Error bars in panels **d-g** represent deviations from the means of at least three replicas.
738

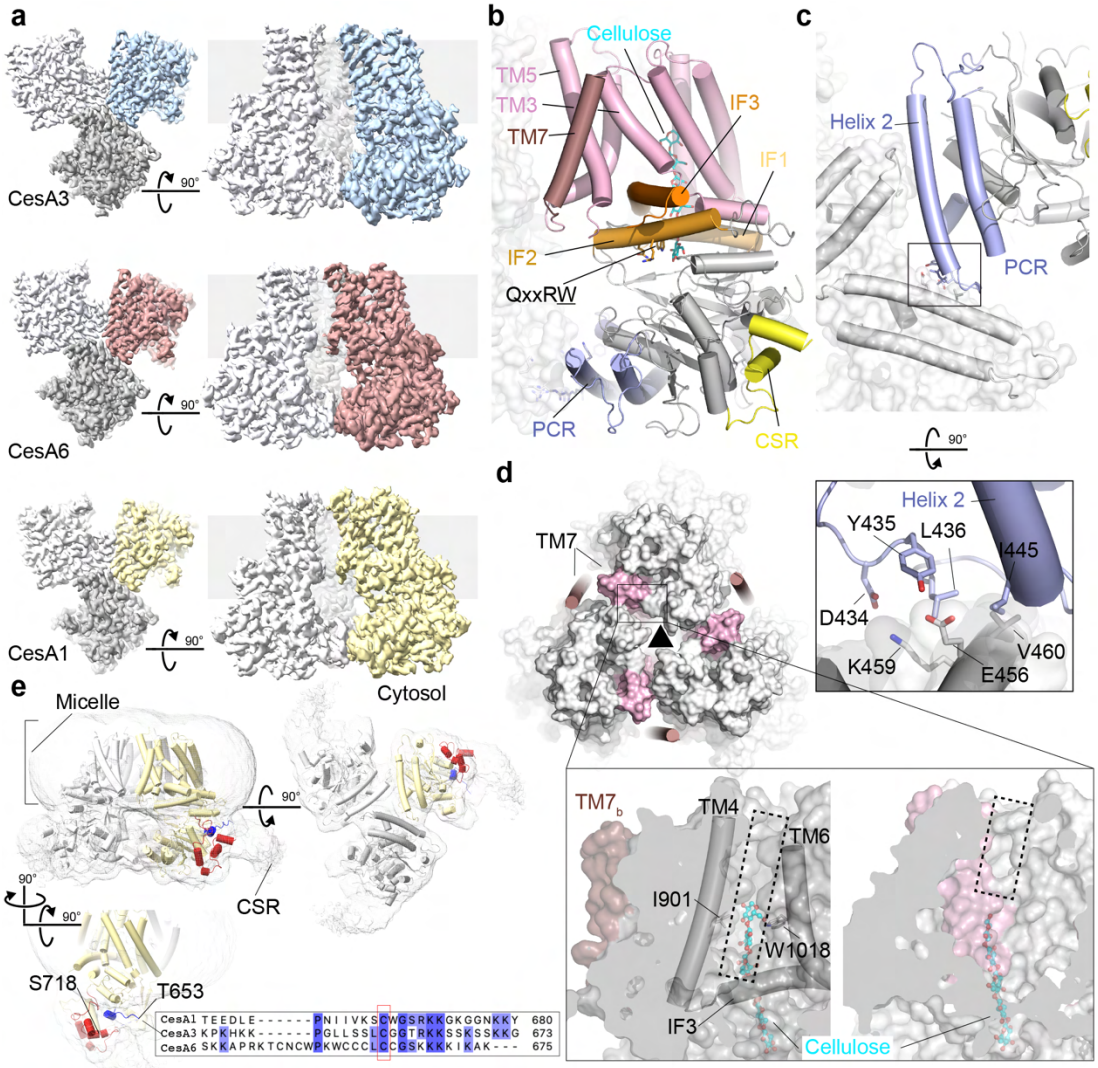

Figure 2. Soybean primary cell wall CesAs assemble into homotrimers. (a) CryoEM maps of the CesA homotrimers contoured at 4.5-5.6 σ. One subunit is shown in color, the others are shown in light and dark gray. The gray background indicates the estimated membrane boundaries. **(b)** Cartoon representation of a CesA6 protomer. The transmembrane region is shown in light and dark pink, interface helices (IF) are shown in orange, and the catalytic domain is colored gray. The PCR and CSR regions are shown in blue and yellow, respectively. **(c)** Cytosolic view of the CesA trimer highlighting the interactions of the PCR domains. **(d)** Comparison of CesA6 and CesA8. Soybean CesA6 is shown as a cartoon and overlaid with hybrid aspen CesA8 (surface, PDB: 6WLB). Transmembrane helix 7 is colored light and dark pink for CesA8 and CesA6, respectively. The black triangle indicates the 3-fold symmetry axis of the homotrimer. Zoom views: Surface representations of CesA6 (left) and CesA8 (right) highlighting the lateral window. $TM7_b$ refers to

752 TM helix 7 of another protomer. **(e)** CryoEM map of the CesA1 trimer shown at a low contour
753 level (1.4 σ). The CesA1 structure is shown as a cartoon with one protomer colored yellow. The
754 resolved CSR N- and C-terminal regions are colored blue and red, respectively. Bottom panel:
755 Sequence alignment of the CSR regions of CesA1, 3 and 6 generated in Clustal Omega ***(Larkin et***
756 ***al., 2007***).
757

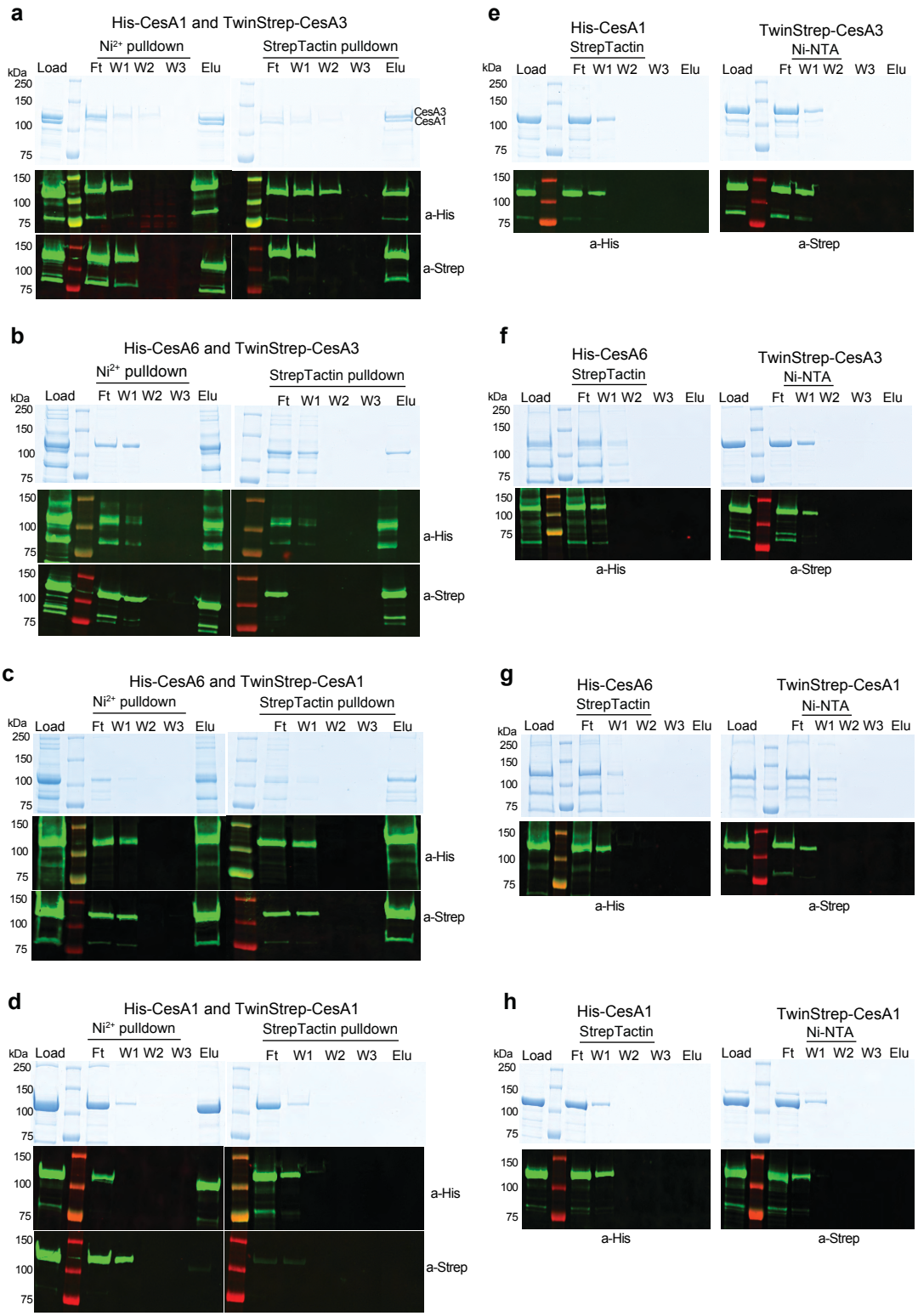

Figure 3. *In vitro* interactions between different CesA isoforms. Tandem pull-down experiments using Ni-NTA and Strep-Tactin resin. Experiments were performed with homotrimers of the

761 indicated CesA isoforms tagged N-terminally either with His- or TwinStrep-tags. Material eluted
762 from the Ni-NTA resin was loaded onto the Strep-Tactin beads. Top panels: Coomassie stained
763 SDS-PAGE, bottom panels: Western blots using anti penta-His or anti-Strep primary antibodies.
764 **(a-c)** Trimer-trimer interactions between CesA1 and CesA3, CesA6 and CesA3, and CesA6 and
765 CesA1, respectively. **(d)** Differently tagged homotrimers of the same isoform do not interact.
766 Tandem purification of a mixture of His- and TwinStrep-tagged CesA1. **(e-h)** Control binding of
767 His-CesAs to Strep-Tactin beads and Strep-CesAs to Ni-NTA resin. F, W, E: Flow through, wash,
768 and eluted fractions.
769

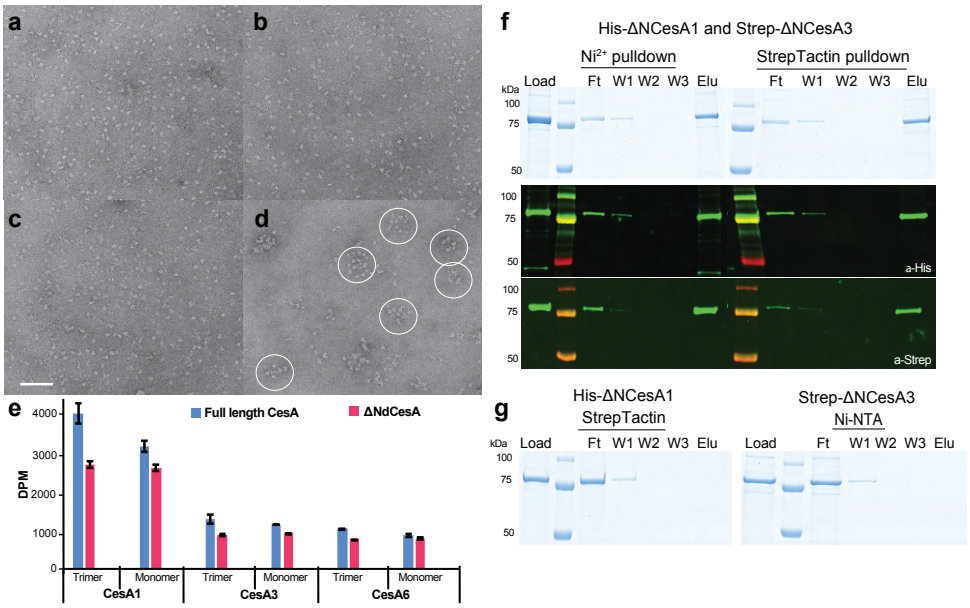

Figure 4. Clustering of CesA homotrimers**. (a-c)** Uranylformate stained EM images of homotrimers of purified GmCesA1 (A), GmCesA3 **(b)** and GmCesA6 **(c)**. The proteins were incubated overnight on ice prior to grid preparation. **(d)** The same for an equimolar mixture of all three CesA isoforms, incubated overnight, separated from individual trimers by size exclusion chromatography, and imaged by negative stain EM. Selected clusters are encircled. Scale bar: 100 nm. **(e-g)** Isoform interactions do not depend on the NTD. **(e)** Activity comparison of full-length and N-terminally truncated CesA isoforms. DPM: disintegrations per minute. **(f)** Tandem pull-down experiments as in ***Figure 3*** but with N-terminally truncated homotrimers of CesA1 and 3. Top panel: SDS-PAGE, bottom panel: Western blots using anti-His and anti-Strep primary antibodies. **(g)** Control binding of His-ΔNCesA1 to Strep-Tactin beads and Strep-ΔNCesA3 to Ni-NTA resin. F, W, E: Flow through, wash, and eluted fractions.

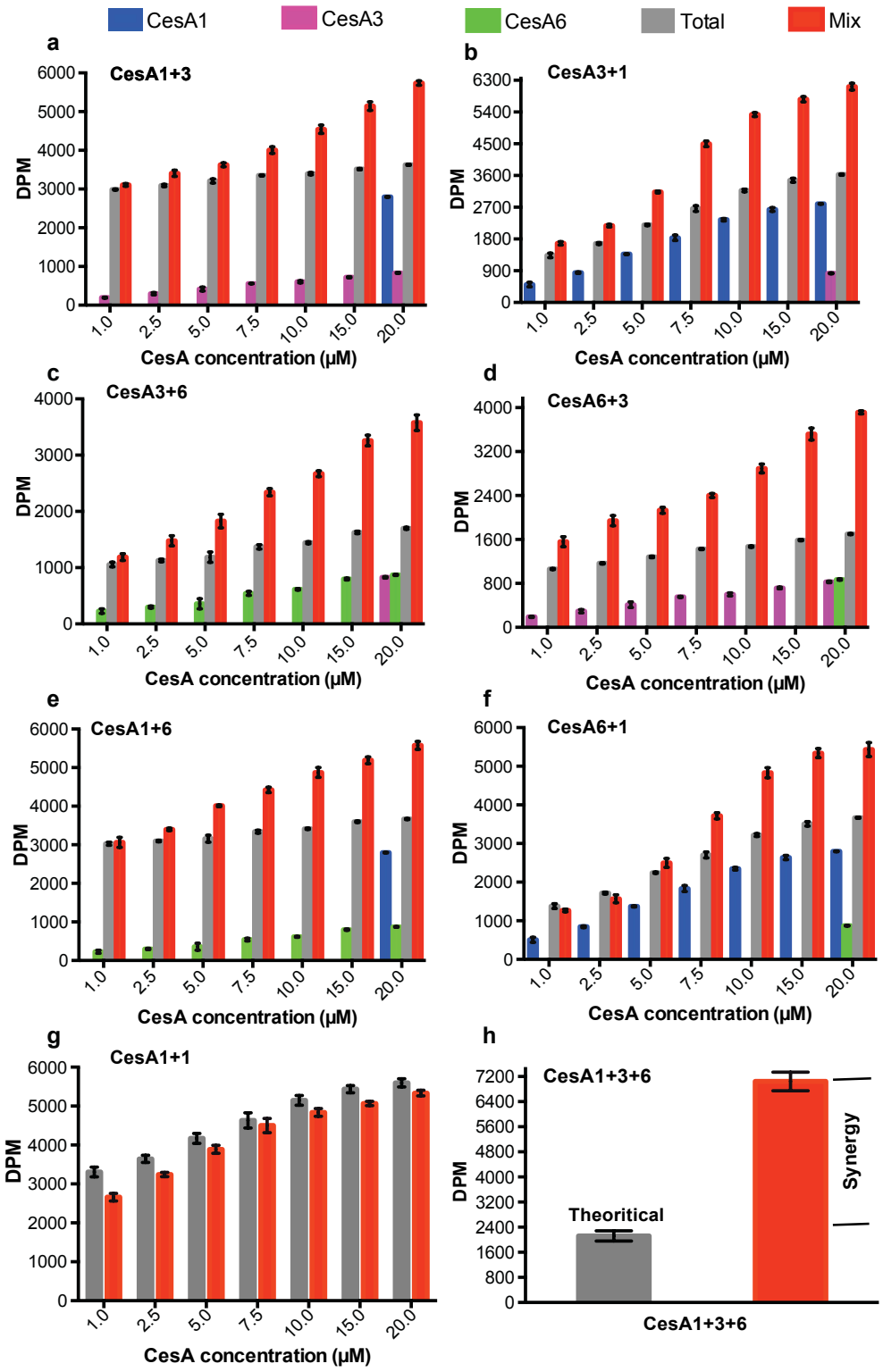

783

784 **Figure 5.** Synergistic catalytic activity. Cellulose biosynthesis from mixtures of CesA isoforms.
785 The formation of ^{3}H-labeled cellulose was quantified by scintillation counting for reaction
786 mixtures containing one CesA isoform at 20 μM concentration and the other isoform at the

787 indicated increasing concentrations. Blue, magenta and green columns represent activities
788 measured for the individual single isoforms alone. Gray columns represent the calculated
789 theoretical activities for the isoform mixtures by adding the individually determined activities. Red
790 columns represent the experimentally determined activities for the isoform mixtures. **(a and b)**
791 $CesA1_{20\ \mu M}$ + $CesA3_{1-20\ \mu M}$ and $CesA3_{20\ \mu M}$ + $CesA1_{1-20\ \mu M}$; **(c and d)** $CesA3_{20\ \mu M}$ + $CesA6_{1-20\ \mu M}$
792 and $CesA6_{20\ \mu M}$ + $CesA3_{1-20\ \mu M}$; and (**e and f**) $CesA1_{20\ \mu M}$ + $CesA6_{1-20\ \mu M}$ and $CesA6_{20\ \mu M}$ + $CesA1_{1-}$
793 $_{20\ \mu M}$, respectively. **(g)** The same as for panel **(a)** but titrating the same CesA isoform ($CesA1_{20\ \mu M}$
794 + $CesA1_{1-20\ \mu M}$). **(h)** The same as for panels a-f but for a combination of all three CesA isoforms.
795 Individual and combined activities were determined at a concentration of 6.6 μM for each CesA
796 isoform. DPM, disintegrations per minute.
797
798

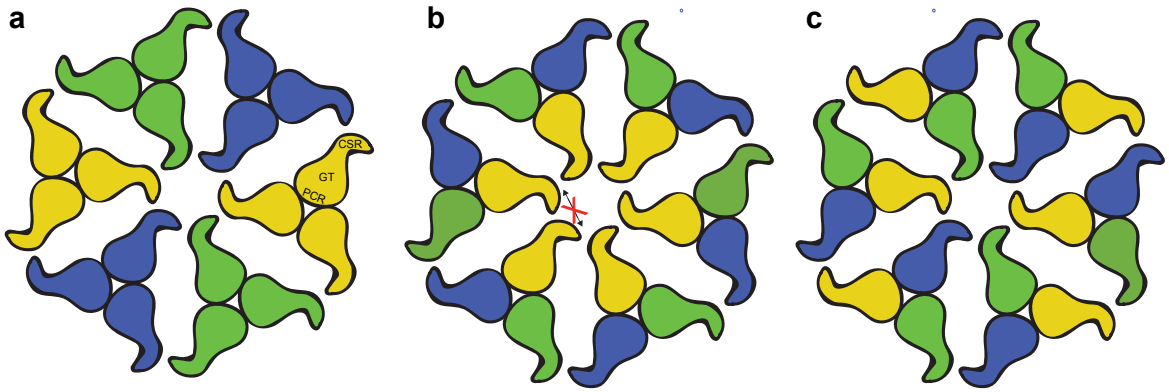

Figure 6. CSC models consisting of different CesA isoforms. **(a)** Association of homotrimers of three different CesA isoforms. Isoforms are indicated by different colors. The shapes represent the cytosolic CesA domains. **(b and c)** CSC assembly from heterotrimeric CesA complexes. Neither heterotrimer formation nor interactions between the same isoforms have been observed *in vitro,* rendering the models less likely. PCR: Plant conserved region, GT: Glycosyltransferase, CSR: Class specific region.